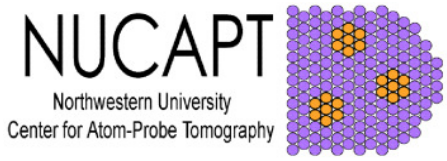

Technion
Israel Institute of Technology

Appendix for Final Report

LEAP Tomography

Figures

Yaron Amouyal – Technion, ISRAEL

Based on:

AMOUYAL, Y. & SEIDMAN, D. N. (2011). An atom-probe tomographic study of freckle formation in a nickel-based superalloy. *Acta Mat.* ***59, 6729-6742.***

AMOUYAL, Y. & SEIDMAN, D. N. (2011). The role of hafnium in the formation of misoriented defects in Ni-based superalloys: An atom probe tomographic study. *Acta Mat.* ***59, 3321 - 3333.***

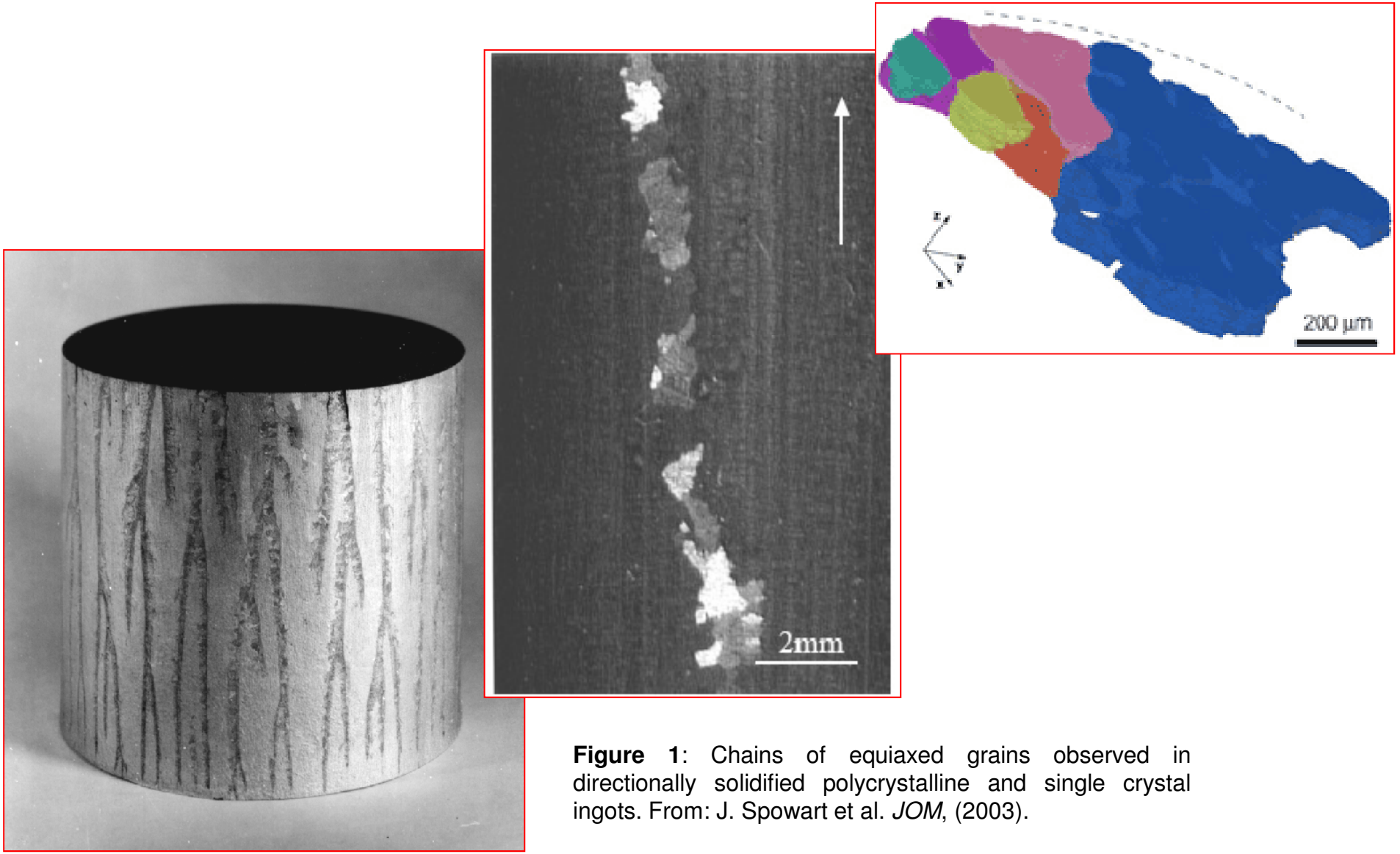

Figure 1: Chains of equiaxed grains observed in directionally solidified polycrystalline and single crystal ingots. From: J. Spowart et al. *JOM*, (2003).

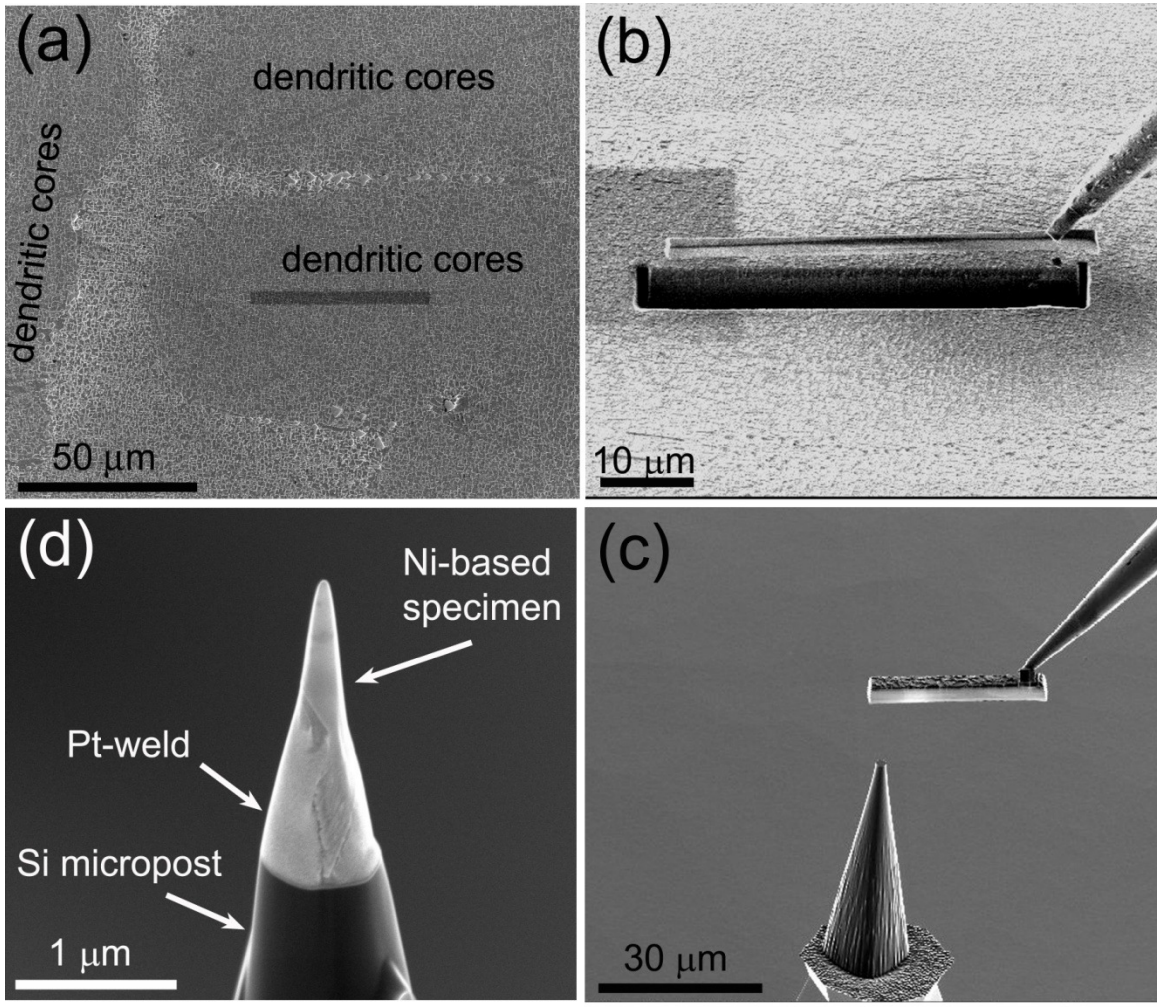

Figure 2. The fabrication procedure for making APT microtips on a Si micropost array utilizing a FEI dual-beam FIB microscope. (a) The dark regions are the dendritic cores in the SC, from which a wedge of alloy is taken. (b) This step involves cutting the wedge and attaching it to a micro-manipulator that lifts it out of the bulk. (c) The wedge is attached to a pre-sharpened Si micropost; and (d) then sharpening the microtip by ion-milling to obtain a 40 nm radius of curvature.

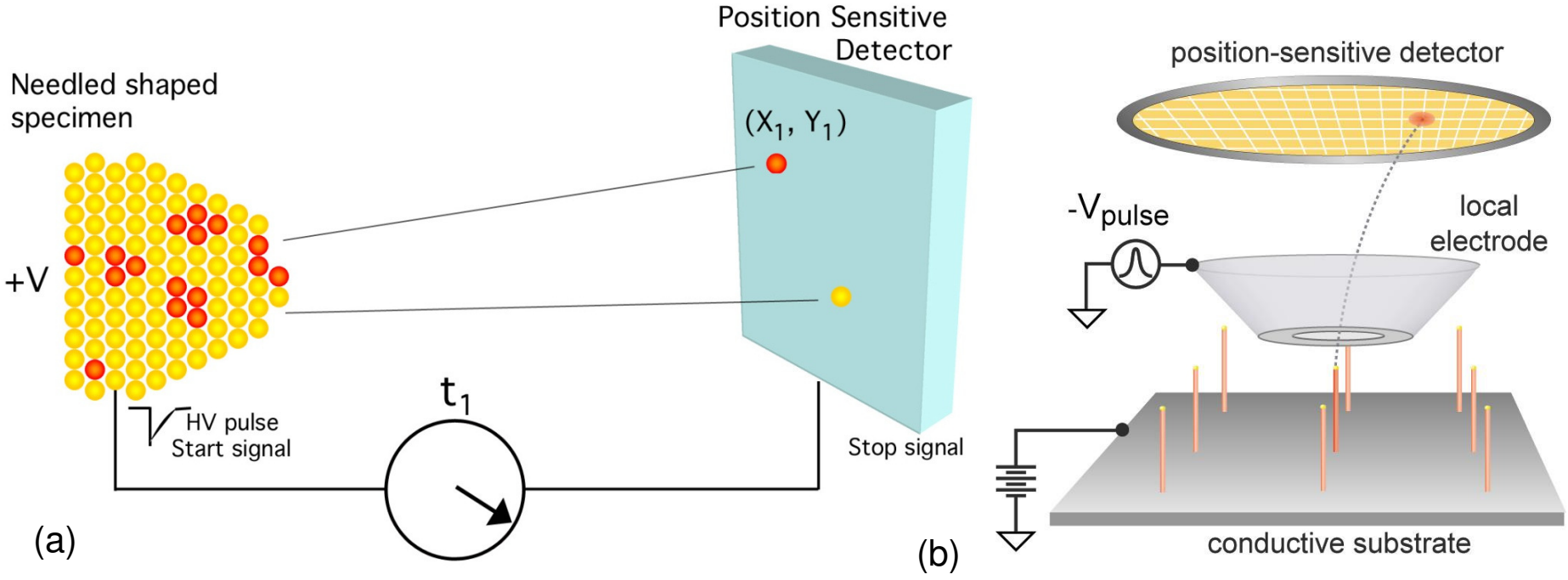

Figure 3. (a) Atom-probe tomography (APT) schematics, with field-evaporation technique, allows atom-by-atom reconstruction of a needle-shaped material containing features of interest. The time-of-flight (TOF) of each field-evaporated ion is measured simultaneously with the position of the impact on the 2D detector, thus the chemical identity of the ion as well as its original location in the specimen are detected. (b) The new configuration of local-electrode atom probe (LEAP) enables a wider field-of-view due to a local-electrode and higher mass resolving power due to laser pulsing.

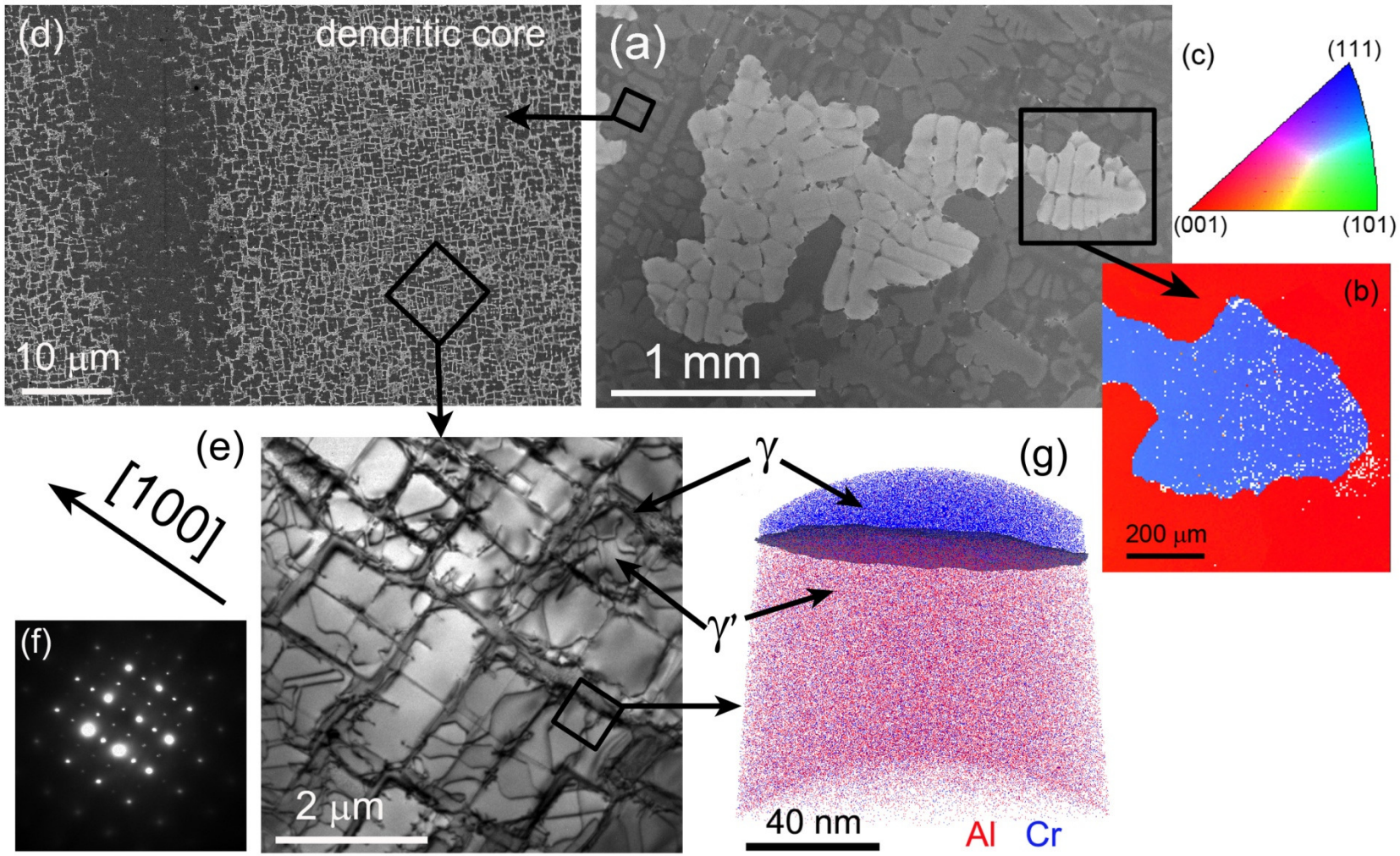

Figure 4. (a) A scanning electron microscope (SEM) image of the cross-section normal to the growth direction showing a freckle (light) on the single-crystal (SC) background (dark). (b and c) An electron back-scattered diffraction (EBSD) pattern of a freckle fragment indicating its preferred {111} surface orientation, appears in blue/dark, while the SC is {100}-oriented, indicated in red/light. (d) A SEM image of the dendritic cores and the inter-dendritic regions in the SC. The dendritic cores are light due to the high volume-fraction of the γ'-phase. (e) A transmission electron microscope (TEM) image along the [001] zone-axis exhibiting a high volume-fraction of cuboidal γ'-precipitates surrounded by thin γ-channels. (f) A selected area electron diffraction (SAED) pattern taken from this area showing that the {100}-faceted precipitates are aligned along the <100>-directions. (g) An atom probe tomographic (APT) reconstruction showing both γ and γ'-phases, represented only by the elements Al (red/light) and Cr (blue/dark), for clarity.

Figure 5. (a) A scanning electron microscopy (SEM) image displaying the four regions of interest (ROIs): the dendritic cores in the single crystal (SC, SC-DC); in the freckles (F-DC); the inter-dendritic regions in the SC (SC-ID); and in the freckles (F-ID). Also presented are 3-dimensional atom-probe tomography (APT) reconstructions of samples lifted-out from the four ROIs: SC-DC (b), SC-ID (c), F-DC (d), and F-ID (e). All APT reconstructions exhibit two-phase γ+γ' microstructures; these phases are identified by the strong partitioning of Cr (blue/dark) to the γ- and of Al (red/light) to the γ'- phase.

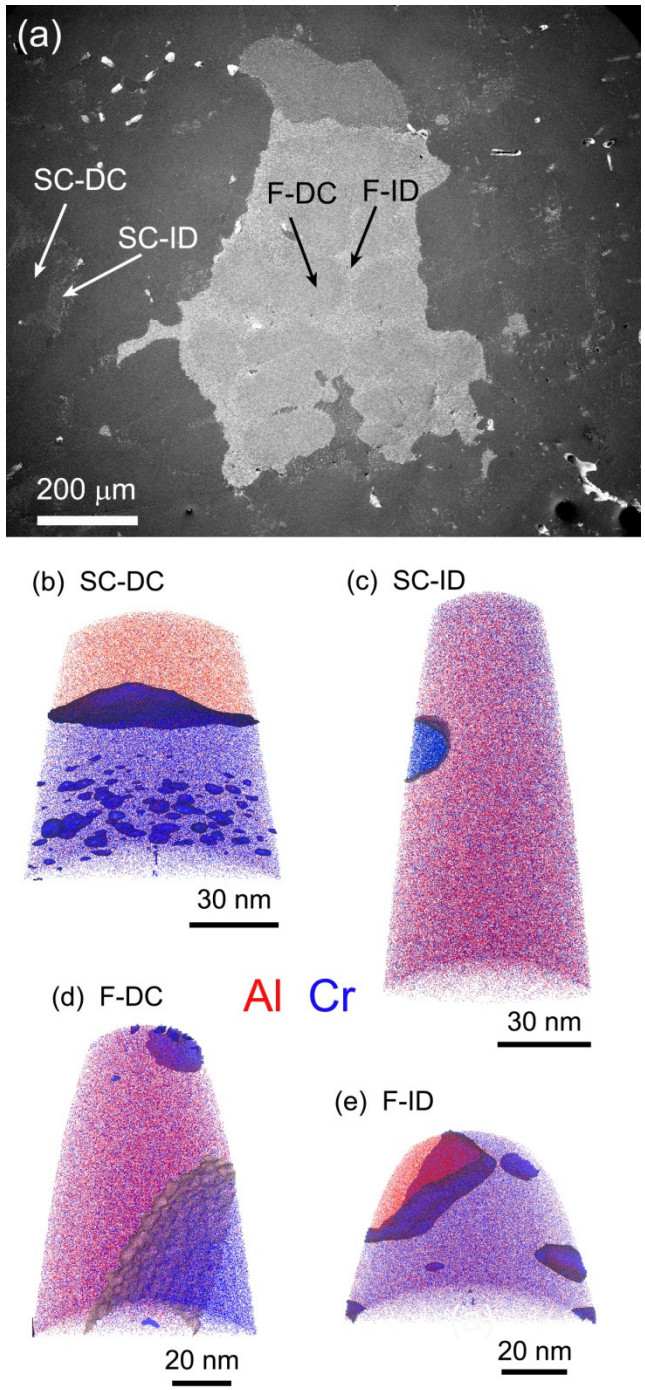

Figure 6. The average concentrations of Al, Cr, Co, Mo, Ta, W, Re, Hf, Fe, and B in the four regions of interest (ROIs) calculated employing the 'lever rule' method, Table 3. Comparison between the concentrations in ROIs SC-ID (green bars) and SC-DC (red bars) indicates that Al, Ta, Fe, Hf, and B partition strongly to the liquid in the single crystal (SC), whereas W and Re unequivocally exhibit solid-phase partitioning. For the freckle, a similar trend is observed comparing ROIs F-ID (cyan bars) and F-DC (blue bars), except for Ta and Fe, which exhibit solid-phase partitioning.

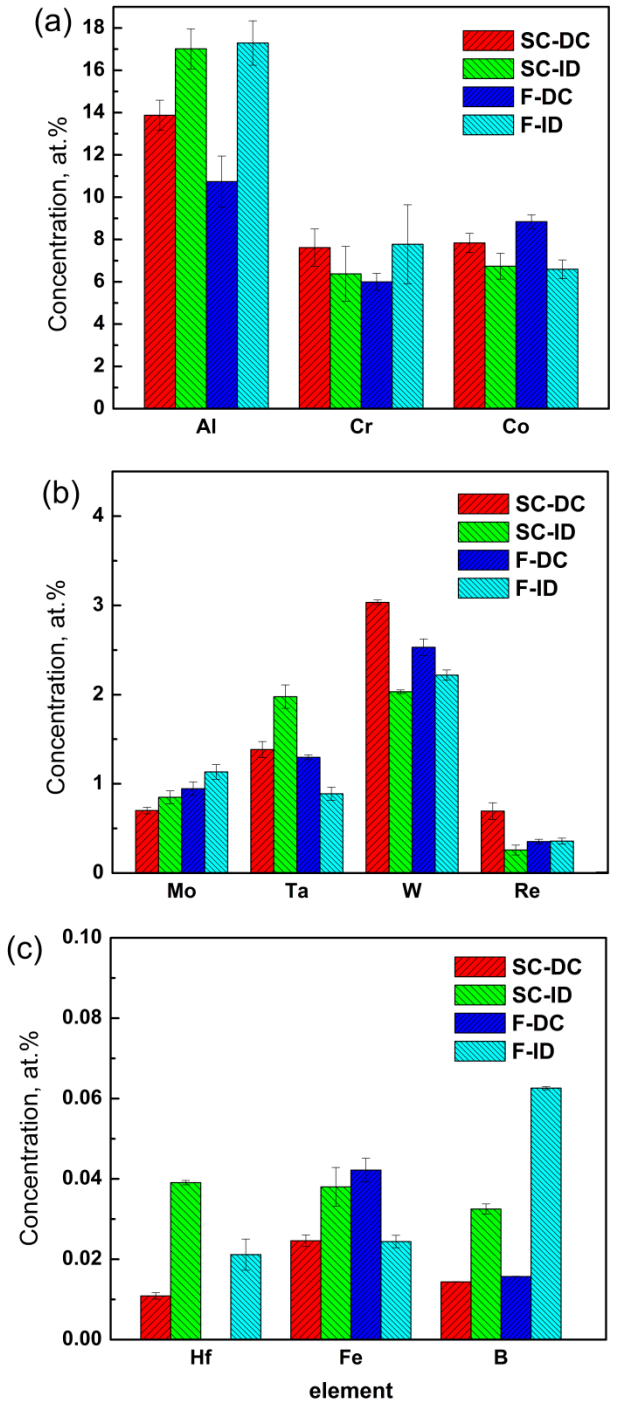

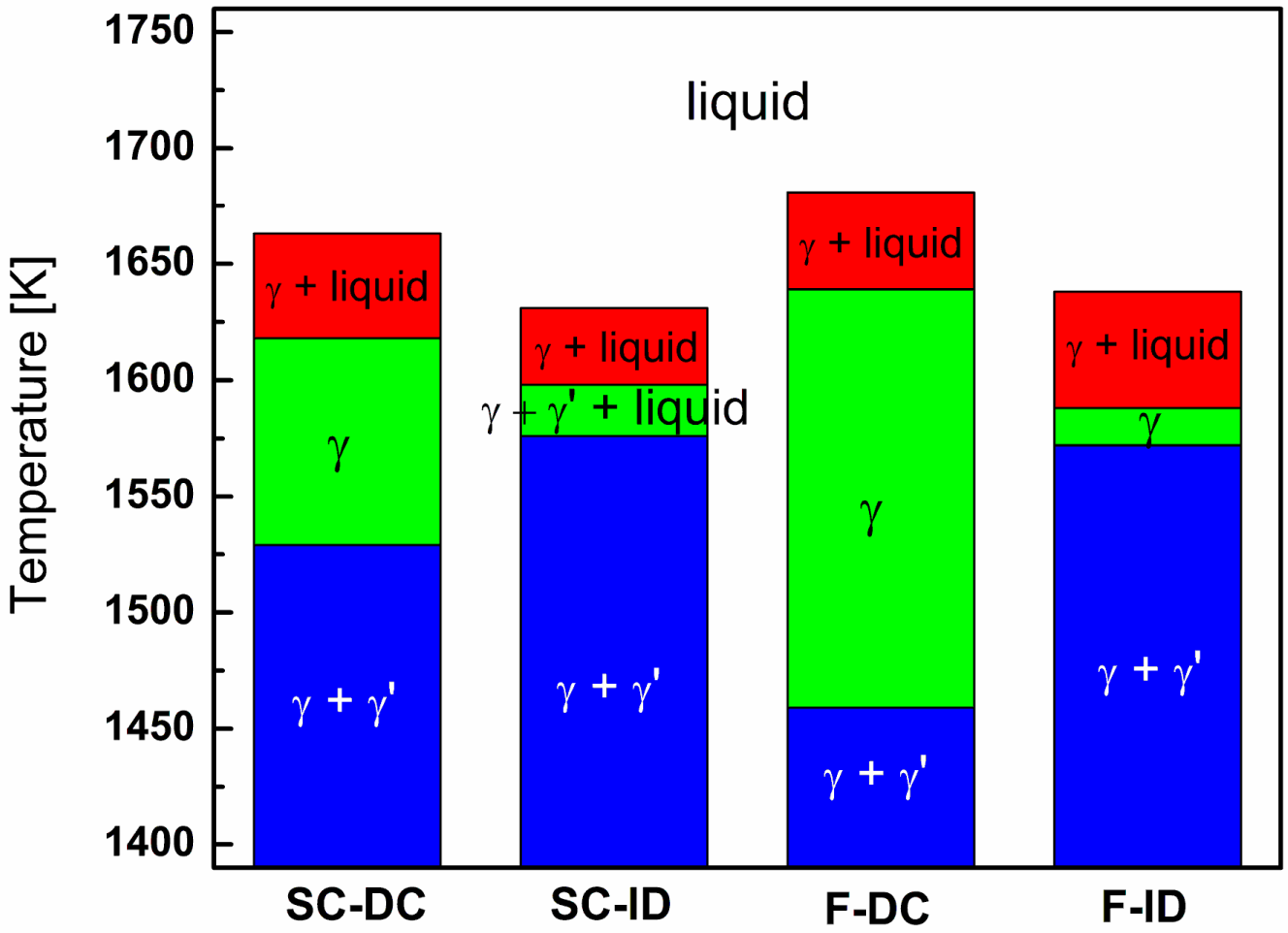

Figure 7. The γ, γ', and liquid phase-fields in the four regions of interest (ROIs) calculated for the average compositions listed in Amouyal & Seidman (2011) using Thermo-Calc. The degree of super-cooling initiating the solidification is inferred from the difference between the γ-liquidus lines for ROIs SC-DC and SC-ID.

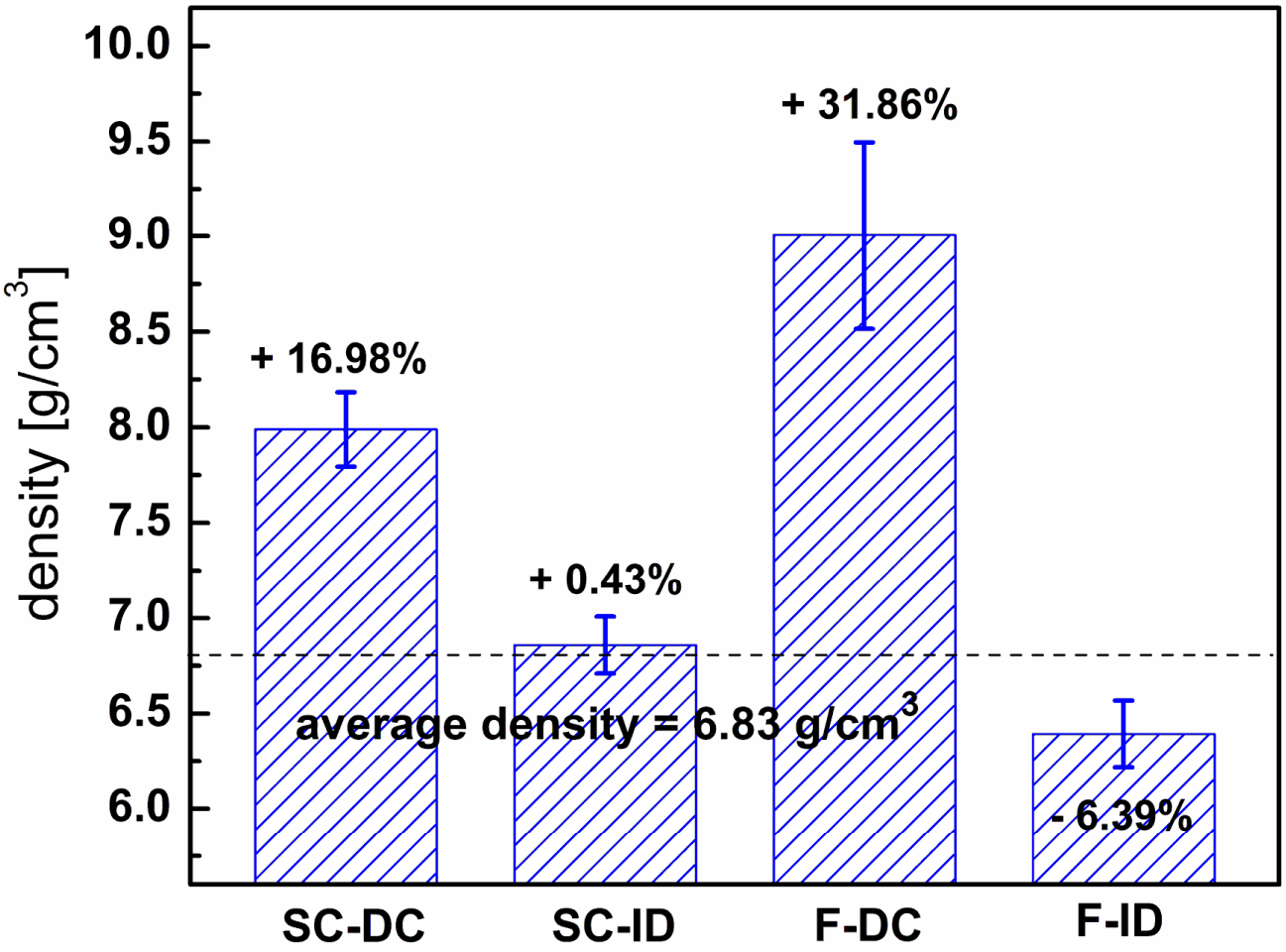

Figure 8. The local densities calculated for regions of interest (ROIs) SC-DC, SC-ID, F-DC, and F-ID based on the average compositions of these ROIs. The horizontal dashed-line represents the average density corresponding to the nominal alloy's composition, and the relative deviations of the local densities from this average value are indicated by numbers.